Measurement of lifetimes and tensor polarizabilities of odd parity states of atomic samarium

S. Rochester[1], C. J. Bowers[1], D. Budker[1,2], D. DeMille[3], and M. Zolotorev[4]

[1]Department of Physics, University of California, Berkeley, CA 94720-7300

[2]Nuclear Science Division, Lawrence Berkeley National Laboratory, Berkeley, CA 94720

[3]Department of Physics, Yale University, New Haven, CT 06520

[4]Center for Beam Physics, Lawrence Berkeley National Laboratory, Berkeley, CA 94720

A systematic measurement of the lifetimes and tensor polarizabilities of the lowest-lying odd parity levels of Sm I was performed. The lifetimes were measured by detecting time-resolved fluorescence following pulsed laser excitation of atoms in an atomic beam; polarizabilities were measured employing the method of Stark-induced quantum beats. An analysis of the data is undertaken to find the best even parity candidate states for an atomic electric dipole moment (EDM) measurement. For the most favorable candidate state ($^7G_1$), the electron EDM enhancement factor is evaluated to be in the range $|R| \approx 100 - 3800$. Critical analysis of the present data along with earlier results in Sm shows the necessity of a term reassignment for several odd parity states. This term reassignment is also used in an estimate of the parity nonconserving $^7F_0 \rightarrow {}^7G_1$ amplitude.

I. INTRODUCTION

In this work, we measured the lifetimes and electric polarizabilities of the lowest-lying odd parity levels of the samarium atom. According to [1], these states have

dominant configuration (Xe)$4f^6 6s6p$ (Fig. 1), while the lowest energy configuration of samarium is (Xe)$4f^6 6s^2$. Lifetimes and electric polarizibilities have been previously measured for only a small number of the energy levels. A recent compilation of previous lifetime measurements in the rare-earth atoms can be found in [2]. Previous tensor polarizability measurements in odd parity states in samarium are presented in [3,4,5,6,7,8,9]. However, to our knowledge, prior to the current work, no systematic study of the lowest odd parity states has been performed.

Fig. 1

The principal motivation for this work is the prospect of an experiment to measure the electric dipole moment (EDM) of the electron by measuring the EDM of a metastable state of samarium. Some of the most sensitive searches for *P*,*T*-violation have been performed in atoms [10]; the best limit on the electron EDM is obtained from an experiment in atomic thallium [11]. It may be possible to improve this limit with EDM searches in metastable states in the rare-earth atoms. In such atoms, there is an enhancement of the atomic EDM due to the proximity of opposite parity levels [12]. In addition, there are potential experimental advantages of states with $J \geq 1$ due to their immunity to certain systematic effects [13,14]. Based on the measurements in this work, an advantageous candidate state for an EDM experiment is selected, and the EDM enhancement factor (ratio of atomic to electron EDM) is estimated.

There are further practical uses for the measurements obtained in this work. A large quantity of accurate atomic data, particularly state lifetimes, is required for analysis

of stellar spectra [15,16]. While rare-earth elements are not prominent in the solar spectrum, they are important for understanding the surface chemistry of upper main sequence stars (chemically peculiar stars) [17]. In addition, rare-earth elements are increasingly used in metal-halide arc lamps to provide high quality and efficient light sources. Spectroscopic data are needed to further development of these lamps [18].

Atomic theory of the rare-earth elements is very complex—thus experimental data is important as a check of the accuracy of calculational techniques. The results of this experiment will be compared to a recent calculation of the lifetimes of several levels of samarium [19].

II. METHOD AND APPARATUS

A block diagram of the setup is shown in Fig. 2. An atomic beam of samarium is intersected at right angles by a linearly polarized, pulsed laser beam tuned to a resonant transition between a particular state of the ground term and the upper state of interest. Following the excitation, the time evolution of fluorescence from the decay back to a particular ground state (not necessarily the same as the initial state) is recorded. To find the decay lifetimes, we fit the observed signals to an exponential. To measure tensor polarizabilities, the method of Stark-induced quantum beats is employed. An electric field is applied to the interaction region, and a particular polarization of the decay fluorescence is monitored. The signal in this case exhibits temporal oscillations—quantum beats—superimposed on the exponential decay. The frequency of the oscillation

is a measure of the tensor polarizability of the state. For general reviews of time-resolved spectroscopy and quantum beats see, e.g., [20] and [21].

Fig. 2

The samarium beam source and the interaction region are contained in a vacuum chamber maintained at a background pressure of about 10^{-6} Torr. The beam oven is a Mo cylinder (2.5 cm diam. $\times$ 7 cm long) with a Mo nozzle at one end and a Ta plug at the other. Tantalum and molybdenum are chosen because they do not react strongly with samarium at high temperatures. The exit nozzle is rectangular, 0.5 cm $\times$ 1.5 cm, and is composed of multiple slits cut with a wire electric discharge machine. The slits are about 0.04 cm wide and 0.6 cm deep, and collimate the atomic beam in the horizontal direction, restricting angular spread to ~0.2 rad.

The oven is resistively heated to ~1200 K, corresponding to a samarium vapor pressure of about 0.2 Torr and an atomic density at the interaction region of $\sim 5 \times 10^{11}$ atoms/cm^3 (consistent with the signal sizes that we measured). Samarium atoms in the beam are thermally distributed among the seven levels of the ground term. At least 1% of the population is in each level. Ten to twenty grams of Sm are loaded into the oven at a time, giving 15 to 30 hours running time. The oven heaters are comprised of coiled Ta wires electrically insulated with high-purity alumina ceramic tubing. Five layers of tantalum foil surround the oven for heat shielding. The total power supplied to the oven is about 100 Watts. To monitor temperature, two sets of (type R) thermocouples are used—one for the body of the oven, and one to measure the temperature at the front of the oven.

The laser used is a tunable dye laser (Quanta Ray PDL-2) pumped by a pulsed Nd-YAG laser (Quanta Ray DCR-2). The laser operates at a 10 Hz repetition rate, with pulses ~8 nsec long. Two dyes were employed: LDS 751 and DCM. Using LDS 751 the dye laser could be tuned in the range 720-763 nm, with a typical output of ~2 mJ per pulse. With DCM, the laser could be tuned in the range 610-673 nm, producing typical output of ~10 mJ. The laser linewidth was ~15 GHz.

The interaction region lies between two plane-parallel electrodes (6.4 cm diam., 1 cm spacing). The polarization of the laser is chosen according to a theoretical optimization as described below. One layer of CO-NETIC AA high permeability alloy surrounds the interaction region, keeping the background magnetic field below 10 mG (see Fig. 3). Holes are cut in the shield to allow the passage of the atomic and laser beams, insertion of the high-voltage cable, and detection of the fluorescence light. Inside the magnetic shield, there is a magnetic coil so that a magnetic field of up to a few Gauss can be applied (parallel to the electric field), in order to analyze possible errors due to residual magnetic fields.

High voltage of up to 40 kV is applied to the top electrode using a novel high-voltage feed-through design (Fig. 3). The high-voltage cable runs through a ceramic stand-off, inside the grounded vacuum chamber, eliminating the possibility of corona discharges. The few discharges that are observed all occur inside the chamber.

Fig. 3

By measuring the plate separation at various points with a telescoping gauge while the vacuum chamber is open to air and adjusting alignment nuts (Fig. 3) as necessary, the high-voltage electrodes can be aligned with each other to within $<10^{-3}$ rad. Absolute spacing is determined with an accuracy of $\sim 3 \times 10^{-4}$ cm.

Fluorescence is detected at 45° to both laser and atomic beams with a 2" diameter photomultiplier tube (PMT, type EMI 9658 with an S-20 Prismatic photocathode). This arrangement is chosen to maximize the Stark-beat signal. The gain of the PMT is $\sim 6 \times 10^5$ and the typical quantum efficiency for the wavelengths used is ~5%. Interference filters are used to select the decay channel of interest, and color glass filters are used to further reduce scattered light from the laser and the oven thermal radiation. Typically, one or two interference filters with bandwidth 10 nm and one or two color glass filters are used. The largest signals were attenuated by putting an aperture or a color glass filter in the laser beam, in order to keep the signal size well within the linear part of the PMT dynamic range. For the Stark-beat measurements, two light polarizations were detected: linear polarization at 45° to the (vertical) electric field direction and a circular polarization. Polaroid film linear and circular polarizers were used in front of the PMT to select these polarizations. The PMT signal is displayed on a Tektronix TDS 410A digitizing oscilloscope, across 50 Ω. The oscilloscope is triggered by the same signal that activates the *Q*-switch of the Nd:YAG laser. Time jitter in the oscilloscope trigger was small compared to the oscilloscope's temporal resolution. Typically, 1000 point-long records at 100 Msamples/sec are taken. Several hundred records corresponding to different laser pulses are averaged. The averaged signal is read out over a GPIB interface to a personal computer running LABVIEW™ data acquisition software.

To reduce the effects of laser light scattered from the vacuum chamber widows, 38 cm-long collimating arms with multiple knife-edge diaphragms are used for the entry and exit of the laser beam. To reduce the effects of light generated by the hot oven, the area around the interaction region was colored black with a permanent marker and an anodized tube was inserted to block oven light not colinear with the atomic beam.

III. DATA COLLECTION AND ANALYSIS

Data collection for both the lifetime and the polarizability measurements is similar. We generally avoid detecting fluorescence light at the same frequency as the excitation pulse because in this case the scattered light from the laser cannot be filtered from the fluorescence. (However, detection at the excitation frequency is unavoidable if the upper state has $J = 0$.) Whenever possible, multiple transition schemes are used for each upper state as a crosscheck of the results. Between one and fifty data files were taken for each upper state. For Stark beats, data files were taken at several values of the electric field to verify the quadratic dependence of the Stark-beat frequency on the electric field.

For each resonance at which data is taken, an off-resonance file is taken, recording the background level, the scattered laser light pulse, and PMT afterpulses and electrical noise associated with the laser pulse. During analysis, the off-resonance file is subtracted from the resonance file to remove these effects from the data (see Sec. V.A).

Lifetime data are modeled by an exponential decay, $s = ae^{-t/\tau} + b$, where a is the signal amplitude, t is time, τ is the state lifetime, and b is the unsubtracted background

signal level. Data are fit to this model with *a*, *b*, and τ as free parameters (Fig. 4). Fitting is started sufficiently long after the excitation pulse time that the effect of the finite PMT response time can be ignored (Sec. V.A).

For Stark-beat data involving an upper state with angular momentum J_e, the model predicts signal of the form

$$s = ae^{-(t-t_0)/\tau}\left(1 + c\sum_{n=1}^{J_e} c_n \cos\left[\frac{3(2n-1)w}{2J_e(2J_e-1)}(t-t_0)+\phi_n\right]\right)+b\,, \tag{1}$$

where the relative contrasts and phases c_n and ϕ_n, $n = 1,..,J_e$, of the series of J_e harmonic frequency components[1], are determined by the density matrix calculation described in Sec. IV. In Eq. (1), t_0 is the beat start time, which should coincide with the laser pulse time, and *c* is a beat contrast (modulation depth) parameter included to account for reduction of contrast due to various effects discussed in Sec.V.C; *c* = 1 corresponds to the contrast predicted by the theory. $w = \frac{\alpha_2 E^2}{\hbar}$, where α_2 is the tensor polarizability, E is the electric field and $\hbar$ is Plank's constant. The six fitted parameters are *a*, *b*, τ, *w*, *c*, and t_0. This model gives adequate fits to all the data (Fig. 5); it was not found necessary, for example, to introduce relative variation in the c_n and ϕ_n.

The uncertainties in the fit parameters are determined as follows. The standard deviation of the background signal before the excitation pulse is used as an estimate of the noise due to dark current and oven light, etc. This uncertainty is combined with an estimate of the shot noise based on the signal size for each data point to estimate the total statistical uncertainty. With this procedure, best fits typically give reduced χ^2 in the range

[1] If J_e is half-integer, there are J_e – ½ frequency components; the index *n* starts at 3/2.

1-10. In an attempt to account for underestimation of the statistical noise in our signals, the calculated uncertainties in the fit parameters (as determined by the square root of diagonal matrix elements of the covariance matrix [22]) are multiplied by the square root of the reduced χ^2. This operation may also help to account for unknown systematic effects since the error is increased if the model fails to reproduce all features of the data.

A discussion of systematic errors and corrections for both lifetime and polarizability measurements is given in Sec. V. To obtain final values, a weighted average is performed of the results from all the data files for each state, with statistical and systematic uncertainties added in quadrature. The uncertainty on the average is multiplied by the square root of the reduced χ^2, if the reduced χ^2 is greater than one. In addition, the final error is made at least as large as the smallest systematic error on any data point. Thus, we adopt a conservative approach in which the uncertainty is made large enough to be compatible with the scattering of the data points, the combined statistical uncertainty of the data points, and the systematic errors on the individual data points.

The extracted lifetimes in the presence of an electric field in general agree with and have comparable uncertainty to the field-free data; thus, lifetime data taken under both conditions are combined.

Fig. 4

Fig. 5

IV. THEORY OF STARK-INDUCED QUANTUM BEATS

An external *z*-directed electric field $\mathcal{E}$ shifts and splits the atomic levels due to the interaction $H_{elec} = -\mathcal{E} d_z$, where d_z is the *z*-component of the dipole moment operator. Second-order perturbation theory gives the energy correction to a state γJM with energy $E_{\gamma J}$ (where M is the *z*-projection of angular momentum J, and γ represents the remaining quantum numbers) due to all other states $\gamma' J' M'$:

$$\Delta E_{\gamma JM} = \mathcal{E}^2 \sum_{\gamma' J'} \frac{\left| \langle \gamma JM | d_z | \gamma' J' M \rangle \right|^2}{E_{\gamma J} - E_{\gamma' J'}}, \tag{2}$$

since the d_z operator only mixes states with the same *z*-projection of total angular momentum. From the Wigner-Eckart theorem and explicit expressions for the appropriate Clebsch-Gordan coefficients [23], we have

$$\langle \gamma JM | d_z | \gamma' J' M' \rangle = \begin{cases} (\gamma J \| d \| \gamma' J') \dfrac{\sqrt{J^2 - M^2}}{\sqrt{J(2J+1)(2J-1)}} & \text{for } J' = J-1,\ M' = M \\ (\gamma J \| d \| \gamma' J') \dfrac{M}{\sqrt{J(J+1)(2J+1)}} & \text{for } J' = J,\ M' = M \\ (\gamma J \| d \| \gamma' J') \dfrac{\sqrt{(J+1)^2 - M^2}}{\sqrt{(J+1)(2J+1)(2J+3)}} & \text{for } J' = J+1,\ M' = M \\ 0 & \text{for } |J' - J| > 1 \text{ or } M' \neq M \text{ or } J = J' = 0, \end{cases} \tag{3}$$

We can write this result in terms of the scalar and tensor polarizabilities (α_0 and α_2, respectively):

$$\Delta E_{\gamma JM} = -\frac{\mathcal{E}^2}{2} \left\{ \alpha_0 + \alpha_2 \frac{3M^2 - J(J+1)}{J(2J-1)} \right\}. \tag{4}$$

In this work, we measure the value of α_2 for the odd parity atomic levels. We then use this value for a given odd parity state to estimate the value of the reduced matrix

element to the nearest even parity "partner" state (with $|J' - J| \leq 1$), assuming that this nearest partner's contribution to the sum in Eq. (2) dominates due to the smallness of the energy-difference denominator. In this case, the tensor polarizability becomes

$$\alpha_2 = \begin{cases} \frac{2}{3}\frac{J(2J-1)\|d\|^2}{\left(E_{\gamma J} - E_{\gamma' J'}\right)}\frac{1}{J(2J+1)(2J-1)} & \text{for } J' = J-1 \\ -\frac{2}{3}\frac{J(2J-1)\|d\|^2}{\left(E_{\gamma J} - E_{\gamma' J'}\right)}\frac{1}{J(J+1)(2J+1)} & \text{for } J' = J \\ \frac{2}{3}\frac{J(2J-1)\|d\|^2}{\left(E_{\gamma J} - E_{\gamma' J'}\right)}\frac{1}{(J+1)(2J+1)(2J+3)} & \text{for } J' = J+1, \end{cases} \tag{5}$$

where $\|d\|$ is shorthand for the reduced matrix element $\left(\gamma J \|d\| \gamma' J'\right)$ to the partner state. Eq. (5) is used to obtain the value of the reduced matrix element from the measured value of α_2. Given this result, we are also interested in the maximum possible projection d_z over all *M*. (This information is used to estimate the EDM enhancement factor.) From Eq. (3) this is given by

$$\left\langle \gamma J M \left| d_z \right| \gamma' J' M \right\rangle_{\max} = \begin{cases} \|d\| \frac{\sqrt{J}}{\sqrt{(2J+1)(2J-1)}} & \text{for } J' = J-1 \\ \|d\| \frac{\sqrt{J}}{\sqrt{(J+1)(2J+1)}} & \text{for } J' = J \\ \|d\| \frac{\sqrt{J+1}}{\sqrt{(2J+1)(2J+3)}} & \text{for } J' = J+1. \end{cases} \tag{6}$$

To calculate the form of the observed signal, we use the density matrix formalism. The general approach is described, e.g., in [24]; details of this particular calculation are given in [25]. The temporal dependence of the intensity of a particular polarization of fluorescence light in a particular direction is given by

$$I \propto \sum_{\substack{MM' \\ m}} \mathrm{F}_{MM'} \mathrm{G}_{MM'} \rho_{mm} e^{-(\Gamma - i\omega_{MM'})(t-t_0)}, \tag{7}$$

where ρ_{mm} is the diagonal ground state density matrix (prior to laser excitation) written in terms of the Zeeman sublevels *m*; Γ is the radiative decay rate of the upper state (inverse of the lifetime);

$$\omega_{MM'} = \frac{3\alpha_2 E^2}{2\hbar}\left(\frac{M^2 - M'^2}{J_e(2J_e - 1)}\right) \tag{8}$$

is the Stark-induced frequency splitting of a given pair of Zeeman sublevels *M*, M' [from Eq. (4)]; t_0 is the time of the laser pulse. (The imaginary parts of the terms in the sum in Eq. (7) cancel each other, so that *I* is real.) $\mathrm{F}_{MM'}$ is the "excitation matrix" given by

$$\begin{aligned} \mathrm{F}_{MM'} &= \left(\gamma_e J_e \| d \| \gamma_g J_g\right)^2 \times \\ &\sum_m \sum_q \sum_{q'} (-1)^{q + J_e - J_g - M - m} e_{(-q)} \left(e_{q'}\right)^* \begin{pmatrix} J_e & 1 & J_g \\ -M & q & m \end{pmatrix} \begin{pmatrix} J_g & 1 & J_e \\ -m & q' & M' \end{pmatrix}, \end{aligned} \tag{9}$$

where $\gamma_g J_g$ is the initial ground state, $\gamma_e J_e$ is the excited state, e_q are the spherical components of the laser polarization vector, and the matrices represent the 3-*J* symbols. The formula for the "detection matrix" $\mathrm{G}_{MM'}$ is identical, except that the ground state J_g is replaced by the final state, J_f, and the laser polarization **e** is replaced by the detection polarization **e′**. When the experimental parameters are specified, the functional form of the signal can be calculated in terms of the quantity $w = \frac{\alpha_2 E^2}{\hbar}$ and the decay rate. For example, in our experimental geometry, with laser and detection polarizations at 45° from vertical, and for $J_g = 2$, $J_e = 2$, $J_f = 1$, we have

$$I \propto e^{-\Gamma(t-t_0)}\left(1+\frac{2\sqrt{2}}{51}\cos\left(\frac{(t-t_0)w}{4}\right)+\frac{12\sqrt{2}}{51}\cos\left(\frac{3(t-t_0)w}{4}\right)\right). \quad (10)$$

In Eq. (10) the tensor polarizability α_2 appears only as the argument of cosine functions. Thus, the sign of α_2 cannot be experimentally determined from Stark-beat data obtained with these experimental conditions. If circularly polarized light is detected, however, α_2 appears as the argument of sine functions, and the sign of α_2 can be determined. The signs of the tensor polarizabilities for the levels for which circularly polarized light was detected are given in the results (Sec. VI, Table II).

Several simplifying assumptions were made in this treatment which could possibly change the contrast (but not the frequency) of the Stark-beats; see Sec.V.C.

A similar treatment gives the form of the signal in the presence of magnetic fields, and combined electric and magnetic fields. Data taken under these conditions were used to confirm the applicability of the theory and to analyze systematic effects.

V. SYSTEMATIC ERRORS

We now turn to a discussion of the various effects that could produce systematic errors in the results. First, effects that alter the signal and could affect the measured values for lifetimes and Stark-beat frequencies are considered. In general, since the Stark-beat measurements are measurements of frequency, they are more robust and are affected much less by distortions of the decay lineshape than the lifetime measurements. Next, issues related to the measurement of the applied electric field are discussed. This was a

dominant source of systematic error for the polarizability measurements. Finally, factors that affect the modulation depth of the observed quantum beats are considered.

A. Lineshape considerations

An optically thick atomic beam increases the apparent radiative lifetime of an excited state due to absorption and re-emission of decay fluorescence. If this effect is present, then the apparent state lifetimes will increase with increasing oven temperature, since samarium vapor pressure and thus the beam density strongly depend on oven temperature. Therefore, measurements at different temperatures for a given upper state were obtained for three states chosen for their strong coupling to the ground state. We see the effect of radiation trapping at the highest beam densities used, but a much less significant effect at lower densities. Using the signal amplitude as an estimate of the atomic beam density, we estimate the absorption coefficient for each data file in order to assess which files are most likely to be affected by radiation trapping. For most states, we see no correlation between the extracted lifetime and the absorption coefficient. However, in some cases, an effect (at a level of up to 5%) is seen, and a correction and associated error is assigned to the lifetime result.

The peak transmission wavelength of an interference filter changes as a function of the angle of incidence. This property, coupled with the change in position of the excited atoms as they fluoresce, could alter the apparent lifetimes. This effect depends on the particular interference filter used to select a given transition, and so can be different for different transitions from the same upper state. A calculation shows that for most data

files, there is less than a 0.1% effect on lifetimes. For the two worst cases, however, the effect is up to 1%, and a correction and error is included for these files. This has no significant effect on the final weighted averages of the lifetimes.

The photomultiplier tube itself introduces certain systematic errors. For many of the transitions studied in our experiment, we were unable to entirely remove the dye laser scattered light pulse from the signal. The scattered light pulse, which can be much larger than the fluorescence signal, can produce afterpulses, which distort the data. Afterpulses are secondary pulses, caused by ionized residual gas in the PMT, which follow a primary anode-current pulse [26]. To remove them from the signal, off-resonance data files are subtracted from the signal files as described above in Sec. III. This cancellation scheme is not perfect, however, since the laser output power can drift between the time the on- and off-resonance files are taken. Thus, some distortion due to afterpulsing may remain in the data files. To estimate the effect of an imperfect cancellation, 10% of the off-resonance file is added to simulated lifetime data (a pure exponential decay) and the resulting data is fit. The difference between the fitted and “true” lifetimes is an estimate of the error due to this effect.

At high signal levels, the response of the photomultiplier tube can deviate from linearity due to space charge effects in the near-anode region. We tested the response of the photomultiplier by measuring scattered-light pulses of different amplitudes from the laser and comparing the peak voltage with the total charge recorded (integral of the PMT signal). Deviation from linearity was modeled with a second-degree polynomial. The model showed that below 50 mV, the effect on the measured lifetime is less than 1%.

Signal levels were much less than 50 mV in almost all cases, so PMT nonlinearity effects should not significantly affect the results.

The PMT used has a response time of about 30 ns FWHM, measured by examining the response of the PMT to a short (~8 ns) scattered light pulse from the dye laser. We have modeled the effect of the finite PMT response time on our fits both analytically and numerically. We find in both cases that the extracted lifetimes are insensitive (within our uncertainties) to the PMT response time τ_{PMT}, as long as τ_{PMT} is much shorter than the fluorescence lifetime and the data are fitted beginning several τ_{PMT} times after the excitation pulse. Typically, we fit data with $t > t_0 + 5\tau_{PMT}$.

It is possible that due to an "accidental" energy coincidence in the complex Sm spectrum a two-photon transition could be excited by the laser light pulse to a level that decays back to the state of interest or to the ground term via some cascade. In this case, the observed fluorescence signal will be the difference of two exponential decays [27], possibly distorting the lifetime fit. We compared the transition frequencies to all known levels with double the transition frequencies employed in this experiment, and found no matches that were allowed by angular momentum selection rules. Many levels in Sm are unknown, so this is not totally conclusive. Therefore, each decay lineshape was examined for anomalies in the temporal evolution; no anomalies were seen. Thus, cascade fluorescence was probably not a factor in any of the lifetime measurements.

Magnetically induced quantum beats (Zeeman beats) can distort the decay lineshape, causing an error in the lifetime or polarizability measurements. A residual magnetic field of ~10 mG, approximately in the *z*-direction, was measured by a Hall-probe inside the mu-metal shield at the interaction region, enough to cause a few percent

error in fitting lifetimes. To estimate this effect for the lifetime measurements, we calculated the beats due to a 10 mG z-directed field for each set of experimental parameters used with a calculation similar to that described in Sec. IV. We generate simulated data with this signal and attempt to fit it with a pure exponential decay. The deviation of the fitted lifetime from the "true" lifetime is used as the estimate of the error due to this systematic effect. A similar procedure is used for the polarizability measurements. Zeeman beat data taken with a z-directed magnetic field of a few gauss supplied by the magnetic coil confirmed the magnitude of the effect for a few transitions.

The samarium sample used has natural isotopic abundance (^{154}Sm: 22.6%, ^{152}Sm: 26.6%, ^{150}Sm: 7.4%, ^{149}Sm: 13.9%, ^{148}Sm: 11.3%, ^{147}Sm: 15.1%, ^{144}Sm: 3.1%). Thus, when a coherently excited state decays, the ~30% of the sample composed of odd mass-number isotopes (with nuclear spin $I = 5/2$) can produce beats due to the hyperfine splitting. The hyperfine structure of some of the levels studied in this work were measured in [28]. The minimum splitting they found was ~100 MHz, which is equal to the digital oscilloscope sampling rate used in this experiment. Assuming the hyperfine splitting is fairly uniform throughout the $4f^6 6s6p$ configuration, hyperfine beats will be too fast to have an effect on the results of our experiment.

In addition to hyperfine beats, the odd isotopes produce Stark-beats. These differ from those produced by the even isotopes, due to the hyperfine structure. To calculate the signal due to these beats, we find the tensor shift for the M_F hyperfine sublevels by writing these states in the basis of the M_J, M_I sublevels. The M_F tensor shift is then the sum of the contributions from the M_J tensor shifts. We use the density matrix calculation to calculate the Stark-beats, using these new tensor shifts. A sum is performed over all

possible hyperfine transitions that can occur during a particular excitation/decay scheme. This calculation showed that the Stark-beats for the odd isotopes have a very low contrast. In the worst case, the Stark-beats would still have <1% expected contrast—not enough to affect fitting of the even isotope Stark-beats, according to our modeling.

When an electric field is applied, lifetimes of the odd parity excited states will change due to admixing of the nearby metastable even parity states. From second-order perturbation theory, for a single close partner, the weight of the partner state admixed is $\sim\left(\frac{\mathbf{d}\cdot\boldsymbol{E}}{\Delta E}\right)^2$. Assuming an infinitely long lifetime for the metastable partner state and small mixing, we have

$$\tau' = \tau\left[1+\left(\frac{\mathbf{d}\cdot\boldsymbol{E}}{\Delta E}\right)^2\right] \tag{11}$$

(for the general formula see Eq. (16), below). For all states measured except for the one at 15650.55 cm^{-1}, this estimate predicts an effect considerably less than 1% even at the highest fields used (~40 kV/cm). For the 15650.55 state, this effect was taken into account when including the lifetimes extracted from the Stark-beat measurements in the lifetime result.

An inhomogeneous electric field will cause atoms at different positions in the interaction region to beat at slightly different frequencies, causing dephasing of the beats. This can affect the lifetime parameter when fitting Stark beats, since the quantum beats will damp out at a faster rate than the exponential decay. This can mimic a shorter lifetime than the true value. The electrodes were aligned so that this effect was insignificant.

B. Electric Field Determination

The high-voltage supplied to the electrodes was measured with a precision voltage divider and a digital voltmeter. We calibrated this output to 0.13% using a high-voltage probe, itself calibrated to 0.1% using a precision voltage source. The uncertainty in the applied voltage was one of the dominant errors in the tensor polarizability measurements.

The high-voltage electrode spacing shifts slightly when the air in the vacuum chamber is pumped out and the chamber lid bends under atmospheric pressure. The top electrode is attached to the center of the chamber lid, and the bottom electrode is attached 5.1 cm from the center. The difference in the deflection between the top and bottom electrode is calculated to be 0.012 mm. This adjustment is included in the determination of the electric field.

C. Quantum-Beat Contrast

We considered various mechanisms that can degrade beat contrast and perturb observed beat phases. Beat contrast varied widely between various measurements, from 20% to 100% of the value predicted by the density matrix calculation. The measured beat start time (overall beat phase) generally agreed with the laser pulse time to within a few percent of the beat period. When the following effects are taken into account, these measurements are in qualitative agreement with expectations.

The ideal polarizer and analyzer orientation in order to produce maximum Stark-beat contrast is calculated according to theory outlined in Sec. IV. However, in the experiment, the orientation of the detection polarizer is set rather crudely, with a 0.1-0.2 rad uncertainty. This could lead to up to a 10% reduction in beat contrast.

Stark-beat contrast resulting from a given laser light pulse depends on the fraction of nuclear spin zero atoms excited. Due to the isotopic abundance and isotope shift, this fraction will vary depending on laser tuning. The isotope shift is measured for some transitions from the ground state to the $4f^6 6s6p$ term in, e.g., [28]. The spectrum of a given transition is a few GHz wide with the two odd isotope resonances occurring at higher frequencies. The dye laser was operated without an intracavity étalon; the radiation linewidth was ~15 GHz, so that a distribution of the isotopes is excited. We measured the contrast of Stark beats as a function of laser tuning near a resonance, showing higher contrast at lower frequencies as expected. The contrast varied from 20-80% over the center part of the resonance; this effect probably accounts for a large fraction of the missing contrast.

Contrast of Stark-beats is affected by the finite PMT and oscilloscope response times (see Sec.V.A). The highest frequency beats are washed out, while lower frequency beats are left unaffected.

In the theoretical development (Sec. IV) we have assumed (by neglecting stimulated emission) weak pumping by the laser light. This is in fact not the case, and two effects due to this—saturation and light shifts due to the AC Stark effect—may affect the signal. These two effects are discussed in the context of quantum beat experiments in [29]. They could conceivably reduce contrast of the quantum beats, change the phase of

the quantum beats, or change the relative contrast or phase of different quantum beat frequency components, but not change the frequency of the beats.

Thus, the combined effect of the above effects is in general agreement with our observations of beat contrast.

VI. RESULTS AND DISCUSSION

The measured lifetimes are given in Table I along with all other lifetimes known to us for samarium levels in the energy range that we examined (below 18,504 cm^{-1}). Measured tensor polarizabilities are given in Table II along with all other tensor polarizabilities of odd parity states in samarium known to us.

Table I

Table II

An *ab initio* calculation of the lifetimes of the lowest-lying odd parity levels of samarium was recently performed using the configuration interaction method [19]. The results are included in Table I. The calculated lifetimes are estimated in [19] to have an uncertainty of 20-30%. A discrepancy of this size between the calculated and experimental values is observed—the theoretical values are generally a factor of ~1.2 higher than those measured in this work. The calculated value of the lifetime of one level,

at 15039.59 cm^{-1}, is particularly high. However, this level was considered for the purposes of the calculation to be part of the ^{9}F term, although, according to [1], it has only 41% of this term. Thus, the calculation for this level would be expected to be less accurate than those for the other levels.

VII. DISCUSSION OF IMPLICATIONS FOR PARITY AND TIME-REVERSAL VIOLATION EXPERIMENTS

We now describe how even parity metastable states of Sm were evaluated as possible candidates for an EDM search. In addition, a term reassignment, prompted by the measurements in this work, of the septet terms of the $4f^6 6s6p$ configuration is proposed. This term reassignment clears up several longstanding discrepancies between theory and experiment in samarium, and may lead to more accurate predictions of *P*- and *T*-odd effects.

Using the measured tensor polarizability, we estimate the dipole coupling **d** to the closest known even parity level, neglecting all other even parity levels. We then determine $|d_z|_{\max}/\Delta E$, where $|d_z|_{\max}$ is the maximum z-projection of **d**, and ΔE is the distance between the opposite parity levels (Table II). The quantity $|d_z|_{max}/\Delta E$ serves as a figure of merit to determine potential even parity candidates for an EDM search (see below). In many cases—especially for the higher-lying levels—one obtains an unreasonably high estimate for the dipole coupling, which makes it likely that there is an unknown close-by state with even parity. These levels are not considered as EDM

candidates for the time being. A search for new even parity levels is currently being undertaken in this laboratory [25]. Given the current experimental knowledge, the most promising state for an EDM search is the metastable even parity $4f^6 5d6s\ ^7G_1$ state at 15639.80 cm^{-1} (designated *X*); its odd parity partner $4f^6 6s6p\ ^7G_1$ state (designated *Y*) is at 15650.55 cm^{-1}. Here, we analyze these states in the context of an EDM experiment—other Sm states may be attractive for EDM experiments as well, as seen from Table II.

In an EDM experiment, atoms are subjected to an external electric field $\boldsymbol{E}$ for a time *t*, and the precession angle

$$\varphi_{\mathrm{EDM}} = \mathbf{d}_{\mathrm{at}} \cdot \boldsymbol{E}\, t = R d_e E\, t \tag{12}$$

($\hbar$ has been set equal to unity) is measured. $\mathbf{d}_{at}$ is the atomic EDM induced by an electron EDM d_e; the electron is exposed to an effective internal field $R\boldsymbol{E}$. In order to maximize the sensitivity to the electron EDM, it is desirable to choose a state with the highest enhancement factor *R* and a sufficiently long lifetime τ, since the latter could be a limiting factor determining *t*. The sensitivity to d_e is determined by the signal-to-noise ratio which in the shot-noise limit is proportional to $\varphi_{\mathrm{EDM}}\sqrt{N}$, where *N* is the number of detected atoms. In a typical atomic beam experiment (such as that of [11]), atoms leaving the atomic beam source pass through three regions. In the first region, alignment is induced in the atomic state under investigation. This alignment then precesses in the second region, in which a strong external electric field is applied. The precession angle is analyzed in the third region. Generally, with a given number of atoms emitted by the source per unit time, the density of atoms in the detection region falls with the distance from the atomic beam source *r* as $1/r^2$. (In principle, the divergence of an atomic beam could be reduced by transverse laser cooling. However, this is exceedingly difficult for

atoms such as samarium due to absence of sufficiently strong closed transitions.) If all the dimensions of the detection volume are $\ll r$ (as is the usual case in practice), and the alignment region is close to the source, then for a state with lifetime τ, $N \propto \exp\left[-r/(\mathrm{v}\,\tau)\right]/r^2$, where v is a typical velocity of atoms in the beam. The signal-to-noise ratio is then proportional to the quantity

$$\varphi_{\mathrm{EDM}}\sqrt{N} = Rd_e E\, t\sqrt{\frac{\exp\left[-r/(\mathrm{v}\,\tau)\right]}{r^2}} = \frac{Rd_e E}{\mathrm{v}}\exp\left[-r/(2\,\mathrm{v}\,\tau)\right]. \qquad (13)$$

For the case of ground state atoms (with $\tau = \infty$), the exponential factor is unity and the signal-to-noise ratio is independent of r. Note that in principle, even if τ is finite, there is no loss in signal-to-noise ratio compared to the case of infinite lifetime, as long as the dimensions of the apparatus are $\lesssim \mathrm{v}\tau$. However, there clearly exists a practical minimum size of the apparatus determined, e.g., by the dimensions of the detection volume and by such experimental considerations as difficulties in placing high voltage electrodes near the hot atomic beam source, a necessity to have heat shields, collisional effects near the source, etc. Setting this size (somewhat arbitrarily) to $r \approx 5$ cm, and using a typical value of thermal velocity of atoms in an atomic beam $\mathrm{v} = 5 \times 10^4$ cm/sec, we get a requirement on the lifetime of the metastable state: $\tau \gtrsim 100$ μsec. Other considerations in the choice of the state include whether there exist convenient ways to populate the state and to produce and probe its alignment, and the sensitivity of the particular state to systematic effects.

We will now discuss various parameters of the states X and Y relevant to an EDM experiment. Let us start with an estimate of the natural lifetime of X. There are seven possible $E1$ decay channels of X; the matrix elements for all are suppressed by the $\Delta S = 0$ selection rule, and the rates are suppressed by small ω^3 phase-space factors, since all

decay wavelengths are in the infrared. Assuming that the amplitudes of these transitions do not exceed ~$ea_0/10$ (a typical value for a spin-suppressed $E1$ matrix element in Sm), where e is the electron charge and a_0 is the Bohr radius, we obtain the lower limit on the lifetime $\tau_X \approx 1$ msec. (The $M1$ and $E2$ transitions to the ground term levels give negligible contribution to the decay rate.)

In the presence of an electric field, there is Stark-mixing between the states of opposite parity. When the electric field is sufficiently high, the lifetime of the Stark-mixed state can be dominated by the admixture of the shorter-lived opposite parity state. Thus the lifetime of state Y is important as well—we have measured it to be 2.626(17) μsec (Table I). The Stark-mixed Zeeman components (with quantization axis chosen along the electric field) can be written as

$$X_{\pm 1} \to X'_{\pm 1} = X_{\pm 1} \pm \frac{\mathbf{d}\cdot\boldsymbol{E}}{\Delta E} Y_{\pm 1}, \tag{14}$$

where $X_{\pm 1}$ and $Y_{\pm 1}$ are the M_J = 1,-1 components of X and Y (there is no Stark mixing for the M_J = 0 component). From Table II we have for the mixing coefficient

$$\frac{\mathbf{d}\cdot\boldsymbol{E}}{\Delta E} \approx \left(1.6\times 10^{-3}\ \text{cm/kV}\right)\boldsymbol{E}\ . \tag{15}$$

For high electric field, the lifetime of the Stark-mixed sublevels with $M_J = \pm 1$

$$\tau_X \to \left[\tau_X^{-1} + \left(\frac{\mathbf{d}\cdot\boldsymbol{E}}{\Delta E}\right)^2 \tau_Y^{-1}\right]^{-1} \tag{16}$$

is dominated by the admixture of the shorter-lived state Y; e.g., at 100 kV/cm, $\tau_X \approx 100$ μsec. Note that the lifetimes are different for sublevels with different $|M|$.

Before proceeding with the estimate of the EDM enhancement factor of the state X, a comment on the structure of the states X and Y is required. These states have been investigated earlier in the context of experiments on P- (not T-) violation [40,36,8]. In

[40] various matrix elements involving X and Y were calculated, including the dipole couplings $\langle X\|d\|Y\rangle\big|_{\text{Ref. [33]}} = 1.7\ ea_0$ and $\langle Y\|d\|G\rangle\big|_{\text{Ref. [33]}} = 3.2\ ea_0$, where G is the ground state. These results, particularly the strong coupling to the ground state, disagree with the experimental data on polarizability (see Table II), radiative transition oscillator strength [35,36,37,38], and the measured lifetime (Table I). (Discrepancy between theory and experiment was first pointed out in [41].) Contradiction between the measured lifetime and theory extends throughout the ^7G term—the experimental lifetimes are between 2.4 and 2.7 μsec, whereas there is ostensibly no suppression of the $E1$ decay channels, according to the designation $4f^6(^7F)6s6p(^1P)\ ^7G$ in [1]. We suggest that the source of all these inconsistencies is that this designation is incorrect. It is clear from the isotope shift data [7,8,28,42] that these states must have core + $6s6p$ dominant configuration. Thus, it is likely that it is the term assignment for the valence electrons that is incorrect. Throughout Ba and the rare earths the core + $6s6p(^1P)$ terms lie 6000-8000 cm^{-1} higher than the core + $6s6p(^3P)$ terms. The levels of the ^7G term appear to have too low an energy for it to be a core + $6s6p(^1P)$ term. These observations indicate that the dominant term of Y must be $4f^6(^7F)6s6p(^3P)\ ^7G$. In fact, the need for this reassignment has been noticed independently by W. C. Martin [43], who pointed out that for all septet terms of this configuration, singlet and triplet valence terms should be interchanged in the tables.

The states X and Y are not pure. State X has dominant term $4f^6(^7F)5d\ (^8G)6s\ ^7G_1$ (58%), with a 22% admixture of $4f^6(^7F)5d\ (^8F)6s\ ^7F_1$. State Y has 79% of its dominant term, and 10% of $4f^6(^7F)6s6p(^3P)\ ^5F_1$ [1]. In addition, state Y has a significant admixture of the configuration $4f^6 5d6p$ (see below). The contributions of each of these components

to the EDM enhancement is evaluated below, but as the relative phases of the components are not known, we presently do not know if the contributions add or cancel.

In order to estimate the EDM enhancement factor, we use the approach described in [44,10]. The electron EDM induces an atomic EDM by mixing states of opposite parity. Assuming that the main contribution comes from the mixing with the state *Y*, the atomic enhancement is given by

$$R = \frac{d_X}{d_e} = \frac{\langle X | d_z/e | Y \rangle}{E_X - E_Y} \langle Y | \varepsilon | X \rangle . \tag{17}$$

Here the first factor indicates the degree of polarization of the atom, and the second the effective electric field acting on the electron when the atom is fully polarized. ε is a single-electron scalar operator with value

$$\left\langle j, l = j \pm 1/2 \left| \varepsilon \right| j, l = j \mp 1/2 \right\rangle = -\frac{16 Z^3 \alpha^2}{\gamma\left(4\gamma^2 - 1\right)\left(\nu_X \nu_Y\right)^{3/2}} \frac{Ry}{a_0}, \tag{18}$$

where $\gamma = \sqrt{\left(j + \frac{1}{2}\right)^2 - Z^2\alpha^2}$, $Z = 62$ is the nuclear charge, α is the fine structure constant, $\nu_X \approx \nu_Y \approx \sqrt{Ry / \left(I.P. - E_{X,Y}\right)} \approx 1.9$ are the effective principal quantum numbers, *I.P.* = 45519 cm^{-1} is the ionization potential, and *Ry* is the Rydberg constant. For the dominant configurations of *X* ($4f^6 5d6s$) and *Y* ($4f^6 6s6p$), this is a single-electron 5*d*-6*p* mixing. The operator ε only connects wavefunctions that are identical except for the *l*-value of a single electron. Writing *X* and *Y* states in terms of wavefunctions for the core and each of the two valence electrons (using the ^3P reassignment of state *Y* as discussed above), we can evaluate this matrix element, introducing the angular coefficient *F* that expresses how much of the states *X* and *Y* are the same except for the mixed electron. The matrix element vanishes for every other component of the states' wavefunctions. Thus,

$$R = -16Fa_{X1}a_{Y1}\frac{Ry}{E_X - E_Y}\frac{\langle X|d_z|Y\rangle}{ea_0}\frac{Z^3\alpha^2}{\gamma\left(4\gamma^2-1\right)\left(\nu_X\nu_Y\right)^{3/2}}, \quad (19)$$

where a_{X1}, a_{Y1} are the amplitudes of the dominant components of X and Y (square root of the probabilities, with sign as yet undetermined), j = 3/2 is the only possible common value of the single-electron total angular momentum for a p and a d state, the experimental value of d_z is taken from Table II, and we have calculated $F \approx$ -0.35.

In addition to the contribution of the dominant configurations, one can also expect a significant effect due to the admixture of the $4f^6 5d6p$ configuration to the state Y. Even a relatively small admixture of this configuration is important, since the 6*s*-6*p* EDM mixing is much stronger than 5*d*-6*p* EDM mixing; this is due to the fact that the main contribution to the EDM matrix element is from the region close to the nucleus. The amplitude of the $4f^n 5d6p$-$4f^n 6s6p$ mixing is known to be ~0.2 throughout the rare earth elements [45]; a similar value was also estimated for Sm [46]. Explicit calculations of 6*s*6*p*-5*d*6*p* configuration mixing have been performed for only a few cases in the rare earths, such as Eu I, Tm II, Yb I, Lu I, and Lu II; these are mentioned, along with the appropriate references, in [1]. In all these cases, the mixing amplitudes are of similar size: ~0.2-0.3 for states identifiable as core + ^3P terms. This systematically constant mixing can be understood in a simple way. The filling of the 4*f* subshell in the rare earths is accompanied by the collapse of the 4*f* orbital radius [47]. Because of this collapse, the effective potential seen by an electron in a valence shell (such as *6s*, 6*p*, or 5*d*) varies only slightly as a function of Z throughout the region from Z = 56 (Ba) to Z = 71 (Lu); this is because each additional nuclear charge is effectively screened by an additional, compact 4*f* electron. This effect is verified by noting that the binding energies of these valence electrons vary only slightly in this range of *Z*. Calculations in [47] also verify the

expected small variation in the mean orbital radii of these valence shells. Since configuration mixing depends only on electrostatic integrals and energy denominators, it is clear that the 6*s*6*p*-5*d*6*p* mixing should be similar throughout the (spectrally complex) rare earths. The value of the mixing can thus be taken from the relatively simple cases of Ba and Yb, where recent calculations were performed [48,49,50]. These mixing amplitudes lie in the general range given above.

Performing EDM enhancement factor estimates similar to the one above for the contribution of the secondary terms of X and Y and the admixture of the $4f^6 5d6p$ configuration, one finds that two contributions are significant in addition to the one above—the mixing of the dominant term of X with the secondary term of Y, and the mixing of the dominant term of X with the dominant term of the $4f^6 5d6p$ admixture to Y, giving the three contributions to the enhancement factor

$$\begin{aligned} R &= R_{dp}(\text{dominant terms}) + R_{dp}(\text{secondary terms}) + R_{sp}(\text{dominant terms}) \\ &\approx \pm 1100 \pm 800 \pm (1300\text{-}1900), \\ &\text{i.e., } |R| \approx 100\text{-}3800. \end{aligned} \tag{20}$$

Thus, the estimated EDM enhancement factor for the state X in samarium is potentially as high as 4×10^3, exceeding the enhancement factor of the ground state of thallium (~600) by several times. Note that since the relative signs of the contributions are not known, they can, in principle, cancel each other. In addition, this estimate relies both on the accuracy of the state designations given in [1], and on the current understanding of configuration mixing in the states X and Y, discussed above; considering the complexity of the Sm spectrum, neither assumption may be completely justified. A more refined *ab initio* calculation is being performed [51] and its preliminary results indicate a possibility of a large EDM enhancement; however, in this calculation, additional configurations in

the state *X*, not considered in the above estimate, give the primary contribution to the EDM enhancement. Thus, additional theoretical analysis is required to confirm the existence of a large EDM enhancement.

As mentioned above, the states *X* and *Y* have been considered for a measurement of atomic parity nonconservation (PNC), since the near-degeneracy of the two states enhances the parity violating mixing due to the weak interaction H_{weak}. A proposal for a PNC experiment was formulated in [40], and preliminary experiments aimed at evaluating the feasibility of such an experiment were carried out in [36]. The PNC-induced $E1$ matrix element for the $G \to X$ transition

$$E1_{\rm PNC} = \frac{\langle X|H_{weak}|Y\rangle}{\Delta E}\langle Y\|d\|G\rangle, \qquad (21)$$

was calculated in [40]; however, apparently due to the reasons described above, the theoretical value of $\langle Y\|d\|G\rangle$ obtained in this calculation was over an order of magnitude too large. Using the formulae given in [52], we can estimate the value of H_{weak} and thus, using an experimental value for $\langle Y\|d\|G\rangle$, the value of $E1_{\rm PNC}$.

Since PNC arises mainly from the contact weak interaction of electrons with the nucleus, H_{weak} mixes primarily *s* and *p* states (see, e.g., [52]). Thus, from [52],

$$\left|\langle X|H_{weak}|Y\rangle\right| = \left|F'\langle s_{1/2}|H_{weak}|p_{1/2}\rangle\right| = \left|iF'\frac{gZ^3R_{rel}\,q}{(\nu_X\nu_Y)^{3/2}}Ry\right| \approx 3\times10^{-13}\ Ry\,. \qquad (22)$$

Here $F' \approx -0.10$ is an angular factor similar to *F*, described above, $g = \left(Gm_e^2\alpha^2\right)/\left(\sqrt{2}\pi\right)$ is the natural scale of atomic *P*-odd effects, *G* is the Fermi weak interaction constant, m_e is the mass of the electron, $R_{rel} = 4\left(a_0/2Zr_0\right)^{2-2\gamma}/\Gamma^2\left(2\gamma+1\right)$ is the relativistic enhancement factor, r_0 is the nuclear radius, Γ is the gamma-function,

$q = 1 - A/(2Z) - 2\sin^2\theta$, $A = 152$ is the atomic number, and θ is the Weinberg angle. This value for $\langle X|H_{weak}|Y\rangle$ is similar to that found in [40] (accounting for a misprint in that paper).

From the oscillator strength measurement in [38] combined with lifetime measurements, the value for the reduced matrix element $\langle Y\|d\|G\rangle = 0.129(3)\ ea_0$ is found. From the formula for the reduced PNC $E1$ matrix element given above, we have $|E1_{\rm PNC}| \approx 4\times10^{-10}\ ea_0$, nearly a factor of 40 smaller than the value obtained in [40]. This amplitude can be compared with that for an analogous transition in Yb, estimated to be $\sim10^{-9}\ ea_0$ [53,54]. (Note that $E1_{\rm PNC}$ in the Cs $6s_{1/2} \rightarrow 7s_{1/2}$ transition, where the most accurate measurements [55] and calculations [56] have been done, is $|E1_{\rm PNC}| \approx 10^{-11}\ ea_0$.)

VIII. CONCLUSION

We have performed a measurement of the lifetimes of 26 of the lowest-lying odd parity levels of samarium and the tensor polarizabilities of 22 of these levels. (Three of the remaining levels had $J = 0$; Stark-beats were not observed in a fourth level.) Typical relative uncertainties of these measurements are 1-3% for lifetimes and <1% for polarizabilities. Many of these values had not been previously measured; agreement with those that had been measured is satisfactory. We have analyzed samarium and found a potential case of advantage for an EDM search. However, further theoretical analysis is needed to determine whether this case is actually viable.

ACKNOWLEDGMENTS

We acknowledge W. C. Martin for his help with reassigning state designations and M. Kozlov for useful discussions. This work has been supported by UC Berkeley Committee on Research and the LBNL Nuclear Sciences Division. One of us (S.R.) is a recipient of the UC Berkeley Undergraduate Presidential Fellowship.

CAPTIONS

FIG. 1. The low-lying configurations of atomic samarium. The rectangles indicate groups of closely spaced energy levels. The diagram also indicates the location of the odd parity levels whose lifetimes and polarizabilities were measured.

FIG. 2. Block diagram of experimental setup.

FIG. 3. Cross-section of chamber showing high-voltage assembly.

FIG. 4. Decay fluorescence at 637 nm with fit used to extract lifetime. The initial ground term state is $4f^6 6s^2\ ^7F_2$, the excited state is $4f^6 6s6p\ ^7F_2$, and the final ground term state is $4f^6 6s^2\ ^7F_3$. The excitation wavelength is 610.6 nm. The initial section of the decay is not fit because of contamination from the laser light pulse and PMT response time. The lifetime of the upper state is measured to be 1.086(16) μsec.

FIG 5. Stark beat data from fluorescence at 639 nm with fit used to extract polarizability and lifetime. The initial ground term state is $4f^6 6s^2\ ^7F_0$, the excited state is $4f^6 6s6p\ ^7G_1$, and the final ground term state is $4f^6 6s^2\ ^7F_0$. The excitation wavelength is 651.1 nm. The applied electric field was 1.433(4) kV/cm. Circularly polarized light is detected. The tensor polarizability of the upper state is measured to be -561.7(11) kHz/(kV/cm)^2; the lifetime is measured to be 2.626(17) μsec.

TABLE I. All determinations of lifetimes of samarium levels below 18,504 cm^{-1}, including present work. The precise level energies, configurations and terms are from tables [1]; however, the valence electron term reassignments described in Sec. VIII have been made where necessary.

TABLE II. All experimental results for tensor polarizabilities of odd parity states of Sm I, including present work. See comments regarding state designations for Table I. The sign of the polarizability is indicated where known; results placed between vertical bars are absolute values—the sign was not experimentally determined in these cases. *Closest Even Parity Neighbors* lists the three closest known even parity states with $\left|J_{even} - J_{odd}\right| \leq 1$ for each odd parity state (taken from [1,38]). The estimate of $||d||$ is based on only the nearest known partner state (see Sec. IV). If the nearest partner state is unknown, (as is often the case) the matrix element estimate will be incorrect. If the closest known state accounts for the sign of the polarizability, the estimate of $||d||$ is given. If the estimate of $||d||$ is physically plausible, the corresponding values of $|d_z|_{max}$ and $|d_z|/\Delta E$ are given.

FIGURES

TOP

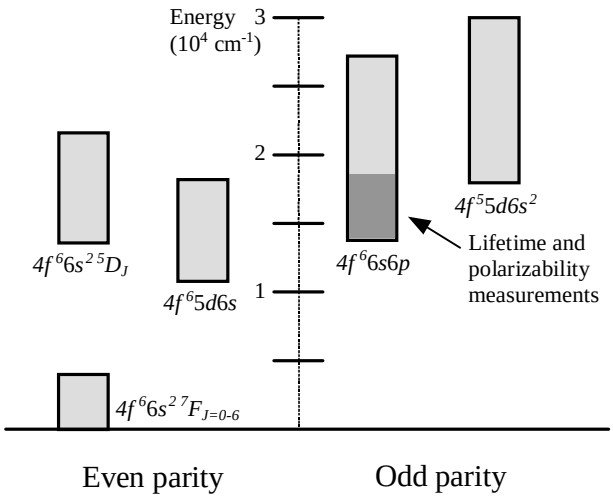

Fig.1. S. Rochester, Phys. Rev. A

TOP

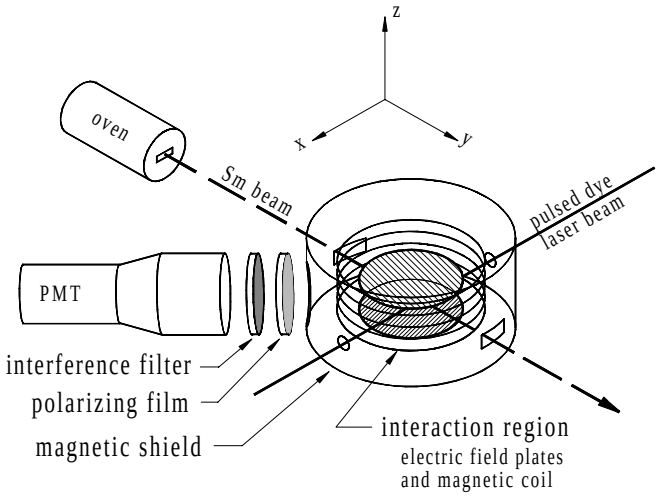

Fig. 2 S. Rochester, Phys. Rev. A

TOP

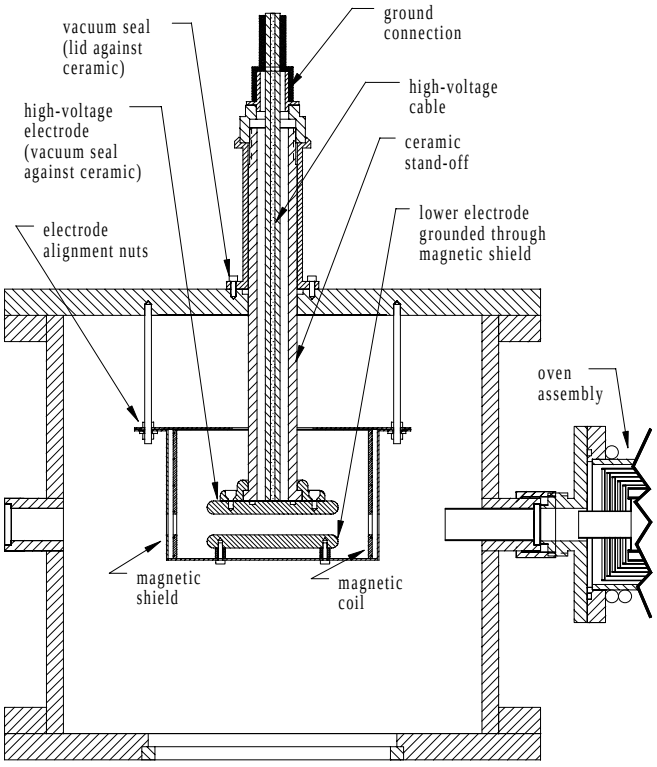

Fig. 3 S. Rochester, Phys. Rev. A

TOP

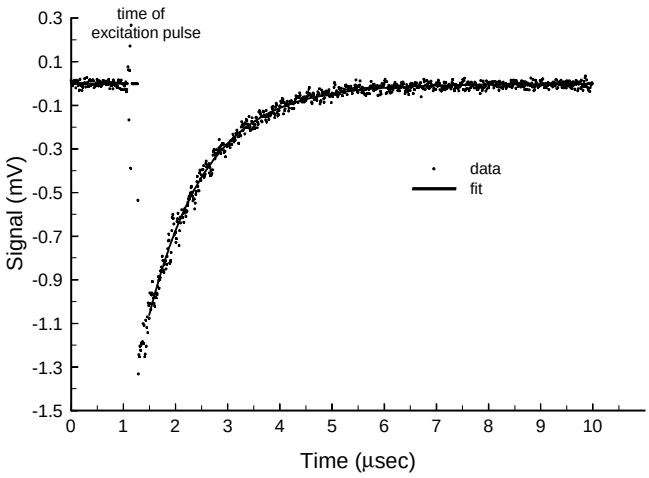

Fig. 4 S. Rochester, Phys. Rev. A

TOP

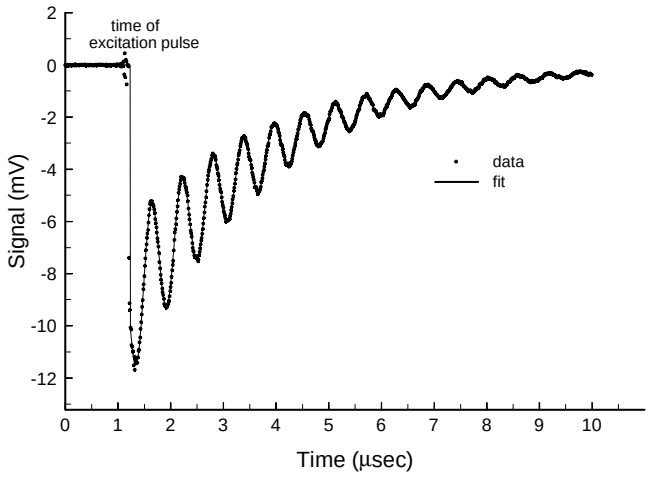

Fig. 5 S. Rochester, Phys. Rev. A

Odd parity state		Lifetime (μsec)						
Energy (cm^{-1})	Leading configuration and term assignment	This work	Previous measurements					Theory
			a	*b*	*c*	*d*	Other	*i*
13796.36	$4f^6(^7F)6s6p(^3P)\ ^9G_0$	3.043(29)						3.2
13999.50	$4f^6(^7F)6s6p(^3P)\ ^9G_1$	2.464(34)						2.9
14380.50	$4f^6(^7F)6s6p(^3P)\ ^9G_2$	2.087(42)						2.6
14863.85	$4f^6(^7F)6s6p(^3P)\ ^9F_1$	0.954(41)						1.2
14915.83	$4f^6(^7F)6s6p(^3P)\ ^9G_3$	1.828(20)						2.4
15039.59	$4f^6(^7F)6s6p(^3P)\ J$=2	1.817(73)						3.4
15507.35	$4f^6(^7F)6s6p(^3P)\ ^9D_3$	2.227(21)						
15567.32	$4f^6(^7F)6s6p(^3P)\ ^9D_2$	2.74(11)						
15579.12	$4f^6(^7F)6s6p(^3P)\ ^9G_4$	1.716(39)						2.4
15586.30	$4f^6(^7F)6s6p(^3P)\ ^5D_0$	2.466(44)						
15650.55	$4f^6(^7F)6s6p(^3P)\ ^7G_1$	2.626(17)					3.3 [e]	
16112.33	$4f^6(^7F)6s6p(^3P)\ ^5D_1$	1.955(40)			1.46(13)			
16116.42	$4f^6(^7F)6s6p(^3P)\ ^7G_2$	2.71(22)						
16131.53	$4f^6(^7F)6s6p(^3P)\ ^9D_4$	2.657(49)						
16211.12	$4f^6(^7F)6s6p(^3P)\ ^9F_3$	4.38(12)						
16344.77	$4f^6(^7F)6s6p(^3P)\ ^9G_5$	1.569(58)						
16681.74	$4f^6(^7F)6s6p(^3P)\ J$=2	1.974(18)				1.70(10)		
16690.76	$4f^6(^7F)6s6p(^3P)\ ^7D_1$		1.71(10)		1.45(20)			
16748.30	$4f^6(^7F)6s6p(^3P)\ ^7G_3$	2.594(96)						
16859.31	$4f^6(^7F)6s6p(^3P)\ ^9D_5$	2.86(22)						
17190.20	$4f^6(^7F)6s6p(^3P)\ ^7F_2$	1.086(16)	1.02(10)		1.20(13)	1.50(10)	1.10(10) [f]	
17243.55	$4f^6(^7F)6s6p(^3P)\ J$=3	1.589(10)				2.22(10)		
17462.37	$4f^6(^7F)6s6p(^3P)\ ^5G_2$				0.122(9)	2.42(10)	1.80 [f]	
17504.63	$4f^6(^7F)6s6p(^3P)\ ^7G_4$	2.420(34)						
17587.46	$4f^6(^7F)6s6p(^3P)\ ^9F_5$	2.66(14)						
17769.71	$4f^6(^7F)6s6p(^3P)\ J$=1		0.157(5)	0.159(10)	0.165(10)		0.038 [g]	
17810.85	$4f^6(^7F)6s6p(^3P)\ ^7F_0$		0.342(10)					
17830.80	$4f^6(^7F)6s6p(^3P)\ ^7F_3$	1.265(11)	1.10(10)			1.58(10)		
18075.67	$4f^5(^6H)5d6s^2\ ^7H_2$		0.450(50)	0.440(40)	0.158(5)		0.480(20) [f]	
18225.13	$4f^6(^7F)6s6p(^3P)\ J$=1		0.146(6)	0.146(8)				
18350.40	$4f^6(^7F)6s6p(^3P)\ ^7G_5$	2.558(79)						
18475.28	$4f^5(^6H)5d6s^2\ ^7F_1$		0.071(2)		0.061(5)		0.069(4) [h]	
18503.49	$4f^6(^7F)6s6p(^3P)\ ^5G_4$	1.471(10)						

[a] Reference [30].
[b] Reference [31].
[c] Reference [3].
[d] Reference [32].
[e] An estimate obtained from measurements in [36,37,38].
[f] Reference [33].
[g] Reference [34].
[h] Reference [35].
[i] Reference [19].

Odd Parity State		Tensor Polarizability [kHz/(kV/cm)^2]		Closest Even Parity Neighbors					Estimate of Matrix Element
Energy (cm^{-1})	Leading configuration And term assignment	This work	Other work	Energy (cm^{-1})	Configuration and term assignment	ΔE (cm^{-1})	$\|\|d\|\|$ (ea_0)	$\|d_z\|_{max}$ (ea_0)	$\frac{\|d_z\|}{\Delta E}$ $\left(10^{-3}\frac{ea_0}{cm^{-1}}\right)$
13999.50	$4f^6(^7F)6s6p(^3P)\ ^9G_1$	|38.89(13)|		14026.45 13732.53 13687.75	$4f^6(^7F)5d(^8F)6s\ ^9F_1$ $4f^6(^7F)5d(^8G)6s\ ^9G_1$ $4f^6(^7F)5d(^8G)6s\ ^9G_2$	26.95 -266.97 -311.75	0.42	0.17	6
14380.50	$4f^6(^7F)6s6p(^3P)\ ^9G_2$	|27.7(12)|		14365.50 14550.50 14612.44	$4f^6(^7F)5d(^8F)6s\ ^9F_2$ $4f^6(^7F)5d(^6P)6s\ ^7P_2$ $4f^6(^7F)5d(^8P)6s\ ^9P_3$	-15.00 170.00 231.94	0.24	0.09	6
14863.85	$4f^6(^7F)6s6p(^3P)\ ^9F_1$	+4.326(9)	+4(1) [a]	14783.51 14550.50 14365.50	$4f^6(^7F)5d(^8D)6s\ ^7D_2$ $4f^6(^7F)5d(^6P)6s\ ^7P_2$ $4f^6(^7F)5d(^8F)6s\ ^9F_2$	-80.34 -313.35 -498.35	0.54	0.20	2
14915.83	$4f^6(^7F)6s6p(^3P)\ ^9G_3$	|27.94(19)|		14920.45 14783.51 14612.44	$4f^6(^7F)5d(^8F)6s\ ^9F_3$ $4f^6(^7F)5d(^8D)6s\ ^7D_2$ $4f^6(^7F)5d(^8P)6s\ ^9P_3$	4.62 -132.32 -303.39	0.14	0.05	10
15039.59	$4f^6(^7F)6s6p(^3P)\ J$=2	|33.179(83)|		14920.45 14783.51 14612.44	$4f^6(^7F)5d(^8F)6s\ ^9F_3$ $4f^6(^7F)5d(^8D)6s\ ^7D_2$ $4f^6(^7F)5d(^8P)6s\ ^9P_3$	-119.14 -256.08 -427.15	1.4	0.40	3
15507.35	$4f^6(^7F)6s6p(^3P)\ ^9D_3$	|77.3(26)|		15524.56 15955.24 14920.45	$4f^6(^7F)5d(^8D)6s\ ^7D_3$ $4f^6(^7F)5d(^8G)6s\ ^7G_2$ $4f^6(^7F)5d(^8F)6s\ ^9F_3$	17.21 447.89 -586.90	0.45	0.15	9
15567.32	$4f^6(^7F)6s6p(^3P)\ ^9D_2$	+24.90(82)		15524.56 15639.80 15834.60	$4f^6(^7F)5d(^8D)6s\ ^7D_3$ $4f^6(^7F)5d(^8G)6s\ ^7G_1$ $4f^6(^7F)5d(^6P)6s\ J$=3	-42.76 72.48 267.28	0.72	0.21	5
15579.12	$4f^6(^7F)6s6p(^3P)\ ^9G_4$	|9.57(21)|		15524.56 14920.45 16354.60	$4f^6(^7F)5d(^8D)6s\ ^7D_3$ $4f^6(^7F)5d(^8F)6s\ ^9F_3$ $4f^6(^7F)5d(^8D)6s\ ^7D_4$	-54.56 -658.67 775.48	0.36	0.09	2
15650.55	$4f^6(^7F)6s6p(^3P)\ ^7G_1$	-561.7(11)	-556(12) [b] -548(12) [c] -563(34) [a] -410(50) [d]	15639.80 15793.68 15914.55	$4f^6(^7F)5d(^8G)6s\ ^7G_1$ $4f^6(^7F)5d(^8F)6s\ ^7F_0$ $4f^6 6s^2\ ^5D_1$	-10.75 143.13 264.00	1.0	0.41	38
16112.33	$4f^6(^7F)6s6p(^3P)\ ^5D_1$	+70.94(31)		15955.24 15914.55 15793.68	$4f^6(^7F)5d(^8G)6s\ ^7G_2$ $4f^6 6s^2\ ^5D_1$ $4f^6(^7F)5d(^8F)6s\ ^7F_0$	-157.09 -197.78 -318.65	3.0		
16116.42	$4f^6(^7F)6s6p(^3P)\ ^7G_2$	-115.23(79)	-112.5(24) [c] -103(10) [a]	15955.24 15914.55 15834.60	$4f^6(^7F)5d(^8G)6s\ ^7G_2$ $4f^6 6s^2\ ^5D_1$ $4f^6(^7F)5d(^6P)6s\ J$=3	-161.18 -201.87 -281.82	1.6	0.58	4

16131.53	$4f^6(^7F)6s6p(^3P)\ ^9D_4$	|76.26(12)|		16354.60	$4f^6(^7F)5d(^8D)6s\ ^7D_4$	223.07			
				15524.56	$4f^6(^7F)5d(^8D)6s\ ^7D_3$	-606.97	1.7	0.52	2
				14920.45	$4f^6(^7F)5d(^8F)6s\ ^9F_3$	-1211.08			
16211.12	$4f^6(^7F)6s6p(^3P)\ ^9F_3$	+3.785(49)		16354.60	$4f^6(^7F)5d(^8D)6s\ ^7D_4$	143.48			
				15955.24	$4f^6(^7F)5d(^8G)6s\ ^7G_2$	-255.88			
				15834.60	$4f^6(^7F)5d(^6P)6s\ J=3$	-376.52			
16681.74	$4f^6(^7F)6s6p(^3P)\ J=2$	|260.09(67)|		15955.24	$4f^6(^7F)5d(^8G)6s\ ^7G_2$	-726.50			
				15834.60	$4f^6(^7F)5d(^6P)6s\ J=3$	-847.14	5.1		
				15639.80	$4f^6(^7F)5d(^8G)6s\ ^7G_1$	-1041.94			
16690.76	$4f^6(^7F)6s6p(^3P)\ ^7D_1$		-13.95(65) [e]	15955.24	$4f^6(^7F)5d(^8G)6s\ ^7G_2$	-735.52			
				15914.55	$4f^6 6s^2\ ^5D_1$	-776.21			
				15793.68	$4f^6(^7F)5d(^8F)6s\ ^7F_0$	-897.08			
16748.30	$4f^6(^7F)6s6p(^3P)\ ^7G_3$	+124.3(26)	+119.8(26) [c] +127(18) [a]	16354.60	$4f^6(^7F)5d(^8D)6s\ ^7D_4$	-393.70			
				15955.24	$4f^6(^7F)5d(^8G)6s\ ^7G_2$	-793.06	4.8		
				15834.60	$4f^6(^7F)5d(^6P)6s\ J=3$	-913.70			
16859.31	$4f^6(^7F)6s6p(^3P)\ ^9D_5$	|129.00(42)|		16354.60	$4f^6(^7F)5d(^8D)6s\ ^7D_4$	-504.71			
				15617.45	$4f^6(^7F)5d(^8H)6s\ ^7H_6$	-1241.86	4.4		
				15082.94	$4f^6(^7F)5d(^8D)6s\ ^9D_6$	-1776.37			
17190.20	$4f^6(^7F)6s6p(^3P)\ ^7F_2$	-25.30(15)	-20.8(15) [e] -23(2) [a]	17864.29	$4f^6 6s^2\ ^5D_2$	674.09			
				18176.17	$4f^6(^7F)5d(^6H)6s\ ^7H_2$	985.97			
				15955.24	$4f^6(^7F)5d(^8G)6s\ ^7G_2$	-1234.96			
17243.55	$4f^6(^7F)6s6p(^3P)\ J=3$	+95.18(31)		17864.29	$4f^6 6s^2\ ^5D_2$	620.74			
				16354.60	$4f^6(^7F)5d(^8D)6s\ ^7D_4$	-888.95			
				18176.17	$4f^6(^7F)5d(^6H)6s\ ^7H_2$	932.62			
17462.37	$4f^6(^7F)6s6p(^3P)\ ^5G_2$		+1315(120) [a]	17864.29	$4f^6 6s^2\ ^5D_2$	401.92			
				18176.17	$4f^6(^7F)5d(^6H)6s\ ^7H_2$	713.80	8.5		
				15955.24	$4f^6(^7F)5d(^8G)6s\ ^7G_2$	-1507.13			
17504.63	$4f^6(^7F)6s6p(^3P)\ ^7G_4$	-5.84(10)		16354.60	$4f^6(^7F)5d(^8D)6s\ ^7D_4$	-1150.03			
				15834.60	$4f^6(^7F)5d(^6P)6s\ J=3$	-1670.03	1.1	0.32	0.3
				15524.56	$4f^6(^7F)5d(^8D)6s\ ^7D_3$	-1980.07			
17587.46	$4f^6(^7F)6s6p(^3P)\ ^9F_5$	+36.20(32)		16354.60	$4f^6(^7F)5d(^8D)6s\ ^7D_4$	-1232.86			
				15617.45	$4f^6(^7F)5d(^8H)6s\ ^7H_6$	-1970.01	3.7		
				15082.94	$4f^6(^7F)5d(^8D)6s\ ^9D_6$	-2504.52			
17769.71	$4f^6(^7F)6s6p(^3P)\ J=1$		+13.13(57) [e] +13.55(6) [f]	17864.29	$4f^6 6s^2\ ^5D_2$	94.58			
				18176.17	$4f^6(^7F)5d(^6H)6s\ ^7H_2$	406.46			
				15955.24	$4f^6(^7F)5d(^8G)6s\ ^7G_2$	-1814.47			
17830.80	$4f^6(^7F)6s6p(^3P)\ ^7F_3$	-202.74(94)		17864.29	$4f^6 6s^2\ ^5D_2$	33.49			
				18176.17	$4f^6(^7F)5d(^6H)6s\ ^7H_2$	345.37	1.1	0.33	10
				16354.60	$4f^6(^7F)5d(^8D)6s\ ^7D_4$	-1476.20			
18075.67	$4f^5(^6H^o)5d6s^2\ ^7H_2$		+9.15(35) [e] +10(1) [a]	18176.17	$4f^6(^7F)5d(^6H)6s\ ^7H_2$	100.50			
				17864.29	$4f^6 6s^2\ ^5D_2$	-211.38	0.36	0.13	1
				20195.76	$4f^6 6s^2\ ^5D_3$	2120.09			

18209.04	$4f^6(^7F)6s6p(^3P)\ ^5G_3$		-150(9) [a]	18176.17	$4f^6(^7F)5d(^6H)6s\ ^7H_2$	-32.87			
				17864.29	$4f^6 6s^2\ ^5D_2$	-344.75			
				16354.60	$4f^6(^7F)5d(^8D)6s\ ^7D_4$	-1854.44			
18225.13	$4f^6(^7F)6s6p(^3P)$ J=1		-6.08(31) [e] -6(1) [a]	18176.17	$4f^6(^7F)5d(^6H)6s\ ^7H_2$	-48.96			
				17864.29	$4f^6 6s^2\ ^5D_2$	-360.84			
				20195.76	$4f^6 6s^2\ ^5D_3$	1970.63			
18416.62	$4f^6(^7F)6s6p(^3P)$ J=2		+9.12(50) [e] +9(4) [a]	18176.17	$4f^6(^7F)5d(^6H)6s\ ^7H_2$	-240.45			
				17864.29	$4f^6 6s^2\ ^5D_2$	-552.33			
				20195.76	$4f^6 6s^2\ ^5D_3$	1779.14			
18503.49	$4f^6(^7F)6s6p(^3P)\ ^5G_4$	-717.2(15)	-660(46) [a]	20195.76	$4f^6 6s^2\ ^5D_3$	1692.27			
				16354.60	$4f^6(^7F)5d(^8D)6s\ ^7D_4$	-2148.89	17		
				15834.60	$4f^6(^7F)5d(^6P)6s\ J=3$	-2668.89			
18788.08	$4f^6(^7F)6s6p(^3P)\ ^7F_2$		-7.69(54) [e] -7.3(5) [a]	18176.17	$4f^6(^7F)5d(^6H)6s\ ^7H_2$	-611.91			
				17864.29	$4f^6 6s^2\ ^5D_2$	-923.79	0.80	0.29	0.5
				20195.76	$4f^6 6s^2\ ^5D_3$	1407.68			
18985.70	$4f^6(^7F)6s6p(^3P)\ ^5F_1$		+473(35) [a]	17864.29	$4f^6 6s^2\ ^5D_2$	-1121.41			
				15955.24	$4f^6(^7F)5d(^8G)6s\ ^7G_2$	-3030.46	21		
				15914.55	$4f^6 6s^2\ ^5D_1$	-3071.15			
19009.52	$4f^5(^6H^o)5d6s^2\ J=2$		+9(6) [a]	18176.17	$4f^6(^7F)5d(^6H)6s\ ^7H_2$	-833.35			
				17864.29	$4f^6 6s^2\ ^5D_2$	-1145.23			
				20195.76	$4f^6 6s^2\ ^5D_3$	1186.24			
19501.27	$4f^6(^7F)6s6p(^3P)\ ^7F_3$		+16(1) [a]	20195.76	$4f^6 6s^2\ ^5D_3$	694.49			
				18176.17	$4f^6(^7F)5d(^6H)6s\ ^7H_2$	-1325.10	1.3	0.43	1
				17864.29	$4f^6 6s^2\ ^5D_2$	-1636.98			
19990.25	$4f^5(^6H^o)5d6s^2\ ^7H_4$		+52(6) [a]	20195.76	$4f^6 6s^2\ ^5D_3$	205.51			
				16354.60	$4f^6(^7F)5d(^8D)6s\ ^7D_4$	-3635.65			
				15834.60	$4f^6(^7F)5d(^6P)6s\ J=3$	-4155.65			
20153.47	$4f^6(^7F)6s6p(^3P)\ ^7F_5$		+809(36) [a]	16354.60	$4f^6(^7F)5d(^8D)6s\ ^7D_4$	-3798.87			
				15617.45	$4f^6(^7F)5d(^8H)6s\ ^7H_6$	-4536.02	30		
				15082.94	$4f^6(^7F)5d(^8D)6s\ ^9D_6$	-5070.53			
20163.00	$4f^6(^7F)6s6p(^3P)\ ^7F_4$		-6(1) [a]	20195.76	$4f^6 6s^2\ ^5D_3$	32.76			
				18176.17	$4f^6(^7F)5d(^6H)6s\ ^7H_2$	-1986.83	0.22	0.06	2
				17864.29	$4f^6 6s^2\ ^5D_2$	-2298.71			
21055.76	$4f^6(^7F)6s6p(^3P)\ ^7F_6$		+313(20) [a]	16392.93	$4f^6(^7F)5d(^8H)6s\ ^7H_7$	-4662.83			
				15617.45	$4f^6(^7F)5d(^8H)6s\ ^7H_6$	-5438.31	29		
				15082.94	$4f^6(^7F)5d(^8D)6s\ ^9D_6$	-5972.82			
21458.89	$4f^6(^7F)6s6p(^3P)\ ^7F_5$		+38(6) [a]	16354.60	$4f^6(^7F)5d(^8D)6s\ ^7D_4$	-5104.29			
				15617.45	$4f^6(^7F)5d(^8H)6s\ ^7H_6$	-5841.44	7.7		
				15082.94	$4f^6(^7F)5d(^8D)6s\ ^9D_6$	-6375.95			
22914.07	$4f^6(^7F)6s6p(^1P)\ ^7G_1$		+4(1) [a]	18176.17	$4f^6(^7F)5d(^6H)6s\ ^7H_2$	-4737.90			
				17864.29	$4f^6 6s^2\ ^5D_2$	-5049.78	4.0		
				15955.24	$4f^6(^7F)5d(^8G)6s\ ^7G_2$	-6958.83			

30753.65	$4f^5(^6H^o)5d6s^2\ J=3$	+535(12) [g]	30755.28	$4f^6(^7F)6s(^8F)7s\ ^7F_3$	1.63			
			31246.30	$4f^6(^7F)6s(^8F)7s\ ^5F_2$	492.65	0.37	0.12	74
			30191.24	$4f^6(^7F)6s(^8F)7s\ ^9F_4$	-562.41			

[a] Reference [6].
[b] Reference [7].
[c] Reference [8].
[d] Reference [5].
[e] Reference [3].
[f] Reference [4].
[g] Reference [9].

[1] W. C. Martin, R. Zalubas, and L. Hagan, *Atomic Energy Levels—The Rare Earth Elements* (National Bureau of Standards, 1978).

[2] K. B. Blagoev and V. A. Komarovskii, Atomic Data and Nuclear Data Tables **56**, 1 (1994).

[3] P. Kulina and R.-H. Rinkleff, Z Phys. A **321**, 15 (1985).

[4] C. Neureiter, R.-H. Rinkleff and L. Windholz, J. Phys. B **19**, 2227 (1986).

[5] I. O. G. Davies, P. E. G. Baird and J. L. Nicol, J. Phys. B. **21**, 3857(1988).

[6] D. Burrow and R.-H. Rinkleff, The Arabian Journal for Science and Engineering **17**, 287 (1992).

[7] T. Kobayashi, I. Endo, A. Fukumi, T. Horiguchi, Y. Ishida, T. Kondo, T. Kuwamoto, N. Minamoto, T. Nakamura, T. Takahashi, Z. Phys. D **39**, 209 (1997).

[8] A. Fukumi, I. Endo, T. Horiguchi, Y. Ishida, T. Kondo, T. Kuwamoto, H. Matsuzaki, T. Nakamura, T. Takahashi, Z. Phys. D **42**, 237 (1997).

[9] T. Kuwamoto, I. Endo, A. Fukumi, T. Horiguchi, M. Iinuma, Y. Ishida, T. Kondo, H. Matsuzaki, T. Nakamura, T. Takahashi, J. Phys. Soc. Jpn. **67**, 1213 (1998).

[10] I. B. Khriplovich and S. K. Lamoreaux, *CP Violation without Strangeness; The Electric Dipole Moments of Particles, Atoms and Molecules*, (Springer-Verlag, 1996).

[11] E. D. Commins, S. B. Ross, D. DeMille, and B.C. Regan, Phys. Rev. A **50**, 2960 (1994).

[12] V. A. Dzuba, V. V. Flambaum, and I. B. Khriplovich, Z. Phys. D **1**, 243 (1986).

[13] M. A. Player and P. G. H. Sandars, J. Phys. B **3**, 1620 (1970).

[14] D. Budker and D. DeMille, "Permanent Electric Dipole Moment in Metastable States of Atoms and Molecules", unpublished (1995).

[15] B. Baschek, Physica Scripta. **T8**, 21 (1984).

[16] E. Biémont, N. Grevesse, P. Hannaford, and R. M. Lowe, Astron. Astrophys. **222**, 307 (1989).

[17] C. R. Cowley, Physica Scripta. **T8**, 28 (1984).

[18] M. E. Wickliffe and J. E. Lawler, J. Opt. Soc. Am. B **14**, 737 (1997).

[19] S. G. Porsev, Phys. Rev. A **56**, 3535 (1997).

[20] W. Demtröder, *Laser Spectroscopy, Basic Concepts and Instrumentation, Second Edition* (Springer-Verlag, Berlin Heidelberg, 1996).

[21] S. Haroche, in *High-Resolution Laser Spectroscopy*, edited by K. Shimoda, (Springer-Verlag, Berlin Heidelberg, 1976).

[22] W. H. Press, B. P. Flannery, S. A. Teukolsky, and W. T. Vetterling, *Numerical Recipes in C* (Cambridge University Press, 1988).

[23] I. I. Sobelman, *Atomic Spectra and Radiative Transitions, Second Edition* (Springer-Verlag, Berlin Heidelberg New York, 1992).

[24] A. Corney, *Atomic and Laser Spectroscopy* (Oxford University Press, 1977).

[25] S. Rochester, Undergraduate Thesis, U. C. Berkeley (1998), http://phylabs.berkeley.edu/budker/.

[26] Philips Photonics, *Photomultiplier Tubes, Principles and Applications* (Philips Photonics); Burle, *Photomultiplier Handbook, Theory, Design, Application* (Burle Industries, Inc., 1980).

[27] C. J. Bowers, D. Budker, E. D. Commins, D. DeMille, S. J. Freedman, A.-T. Nguyen, S.-Q. Shang and M. Zolotorev, Phys. Rev. A **53**, 3103 (1996).

[28] H. Brand, B. Nottbeck, H. H. Schulz, and A. Steudel, J. Phys. B **11**, L99 (1978).

[29] M. P. Silverman, S. Haroche, and M. Gross, Phys. Rev. A **18**, 1507 (1978).

[30] P. Hannaford and R. M. Lowe, J.Phys. B **18**, 2365 (1985).

[31] V. N. Gorshkov, V. A. Komarovskii, and N. P. Penkin, Opt. Spectrosc. (USSR) **59**, 268 (1985).

[32] B. B. Krynetskii and V. A. Mishin, Preprint Gen. Phys. Inst. (AN USSR) Rep. **24**, 59 (1990).

[33] P. Hannaford and R. M. Lowe, Austr. J. Phys. **39**, 829 (1986).

[34] H. Brand, K. H. Drake, W. Lange, and J. Mlynek, Phys. Lett. A **75**, 345 (1980).

[35] K. B. Blagoev, V. A. Komarovskii, and N. P. Penkin, Opt. Spectrosc. (USSR) **42**, 238 (1977).

[36] I. O. G. Davies, P. E. G. Baird, P. G. H. Sandars, and T. D. Wolfenden, J. Phys. B. **22**, 741 (1989).

[37] N. P. Penkin and V. A. Komarovskii, J. Quant. Spectrosc. Radiat. Transfer **16**, 217 (1976).

[38] D. M. Lucas, D. N. Stacey, C. D. Thompson, and R. B. Warrington, Phys. Scripta **T70**, 145 (1997).

[39] L. M. Barkov, M. S. Zolotorev and D. A. Melik-Pashaev, Opt. Spektrosk. **66**, 495 (1989) [Opt. Spectrosc. (USSR) **66**, 288 (1989)].

[40] A. Gongora and P. G. H. Sandars, J. Phys. B **19**, 291 (1986).

[41] R. Peterkop, Phys. Lett., **90A**, 182 (1982).

[42] P. Brix, Z. Phys. **126**, 431 (1949); A. R. Striganov, V. A. Katulin, and V. V. Eliseev, Opt. Spectrosc. **12**, 91 (1962); J. E. Hansen, A. Steudel, and H. Walther, Z. Phys. **203**, 296 (1967); J. Bauche, R.-J. Champeau, and C. Sallot, J. Phys. B **10**, 2049 (1977); W. J. Childs, O. Poulsen, and L. S. Goodban, Phys. Rev. A **19**, 160 (1979); M. Wakasugi, T. Horiguchi, W.G. Jin, H. Sakata, and Y. Yoshizawa, J. Phys. Soc. Jpn. **59**, 2700 (1990).

[43] W. C. Martin, private communication (1998).

[44] V. V. Flambaum, Yad. Fiz. (Sov. Nuc. Phys.) **24**, 383, (1976).

[45] J.-F. Wyart and P. Camus, Phys. Scr. **20,** 43 (1979).

[46] S. G. Porsev, Phys. Rev. A **56**, 3535 (1997).

[47] S. A. Kotochigova and I. I. Tupizin, J. Phys. B **20**, 4759 (1987).

[48] J. Migdalek and W. E. Baylis, J. Phys. B **24**, L99 (1991); Phys. Rev. A **33**, 1417 (1986).

[49] S. G. Porsev, Yu. G. Rakhlina, and M. G. Kozlov, Pis'ma Zh. Eksp. Teor. Fiz. **61**, 449 (1995) [JETP Lett. **61** 459 (1995)].

[50] B. P. Das, Phys. Rev. A **56**, 1635 (1997).

[51] M. Kozlov, private communication (1998).

[52] I. B. Khriplovich, *Parity Nonconservation in Atomic Phenomena* (Gordan and Breach, 1991).

[53] D. DeMille, Phys. Rev. Lett. **74**, 4165 (1995).

[54] S. Porsev, Yu. Rakhlina, and M. Kozlov, JETP Lett. **61**, 459 (1995); B. P. Das, Phys. Rev. A **56**(2), 1635 (1997).

[55] C. S. Wood, S. C. Bennett, D. Cho, B. P. Masterson, J. L. Roberts, C. E. Tanner, and C. E. Wieman, Science **275**, 1759 (1997).

[56] V. A. Dzuba, V. V. Flambaum, and O. P. Sushkov, Phys. Lett. **141A**, 147 (1989); S. A. Blundell, W. R. Johnson, and J. Saperstein, Phys. Rev. Lett. **65**, 1411 (1990); Phys. Rev. D **45**, 1602 (1992).